J. Fluid Mech. (1992), *vol.* 239, *pp.* 359–381
Printed in Great Britain

A study of fast dynamo action in chaotic helical cells

By I. KLAPPER

New York University, Courant Institute of Mathematical Sciences, 251 Mercer Street, New York, NY 10012, USA

(Received 24 July 1991)

Fast dynamo action in a chaotic time-periodic flow is investigated. Chaotic motion is created by perturbing a spatially periodic array of helical cells similar to Roberts' cells, leading to an identifiable stretch–fold–shear fast dynamo mechanism. Using the stochastic Wiener bundle method to treat diffusion exactly, numerical results are presented suggesting fast dynamo action. A new numerical method for modelling the role of small magnetic diffusivity is introduced and results are compared with those calculated using the Wiener bundle method. Implications for the role of diffusion in the fast dynamo process are investigated. Finally the relation of the new method to a previously used 'flux growth' method are discussed.

1. Introduction

It has been known for many years that the sun has an active magnetic field. Despite the fact that the age of the sun has not yet reached an ohmic decay time, it is widely believed that the motions of conducting fluid in the solar interior are responsible for the vigour and oscillatory nature of its magnetic phenomena. Growth and maintenance of a magnetic field by fluid process is called dynamo action. In the case of the sun characteristic field evolution times involved are not on the slow diffusive timescale but on rapid advective ones (such as those associated with convective eddies). Such dynamos are called fast (Vainshtein & Zeldovich 1972). In fact the implicit use of fast dynamo action is common in models of astrophysical dynamos because many such models build in magnetic field evolution on advective timescales by choosing an alpha effect (the regenerative mechanism for a poloidal field) independent of diffusivity (see e.g. Roberts & Soward 1992 and references therein). This is despite the fact that the existing theory on which the alpha effect is based relies directly on diffusivity. Similar remarks apply to the theory of turbulent diffusivity. Thus it is important to verify the existence of fast dynamos and understand how they function. One area of recent study is chaotic fast dynamo action (for example Bayly & Childress 1988, 1989; Finn & Ott 1988; Finn *et al.* 1989, 1991; Gilbert 1991, 1992). Chaotic systems are of interest in dynamo theory for their stretching properties which are conducive to magnetic field growth.

By combining Maxwell's equations (but following the standard MHD practice of omitting the displacement current $\partial E/\partial t$) and Ohm's law, it is possible to derive the magnetic induction equation

$$\frac{\partial \boldsymbol{B}}{\partial t}+\boldsymbol{u}\cdot\nabla\boldsymbol{B}=\boldsymbol{B}\cdot\nabla\boldsymbol{u}+R_{\mathrm{m}}^{-1}\nabla^2\boldsymbol{B},\quad \nabla\cdot\boldsymbol{B}=0, \tag{1}$$

where $R_m \equiv UL/\mu = l_{adv}^2/l_{diff}^2$ and η is the magnetic diffusivity. The kinematic approximation, made use of throughout this paper, consists of prescribing a velocity field $\boldsymbol{u}$ such that $\nabla \cdot \boldsymbol{u} = 0$, making (1) a linear equation for $\boldsymbol{B}$. If, given $\boldsymbol{u}$ and smooth initial conditions $\boldsymbol{B}_0(\boldsymbol{x}) \equiv \boldsymbol{B}(\boldsymbol{x}, 0)$, the magnitude of the solution $\boldsymbol{B}$ of equation (1) exhibits exponential growth at a rate $p(R_m) > 0$ for some R_m then $\boldsymbol{u}$ is a kinematic dynamo. If, in addition,

$$\overline{\lim}_{R_m \to \infty} \left(\sup_{B_0} p(R_m) \right) > 0, \tag{2}$$

then in some sense the growth is independent of diffusion and $\boldsymbol{u}$ is called a kinematic fast dynamo. Of course, the kinematic approximation ignores coupling between $\boldsymbol{B}$ and $\boldsymbol{u}$. In the fully nonlinear problem a strong magnetic field would, through the Lorentz force $\boldsymbol{J} \times \boldsymbol{B}$, eventually alter $\boldsymbol{u}$ in such a way as to halt growth. This aspect of the dynamo problem will not be considered here.

By setting $R_m = \infty$, (1) reduces formally to

$$\frac{\partial \boldsymbol{B}}{\partial t} + \boldsymbol{u} \cdot \nabla \boldsymbol{B} = \boldsymbol{B} \cdot \nabla \boldsymbol{u}, \quad \nabla \cdot \boldsymbol{B} = 0. \tag{3}$$

This equation has the well-known Cauchy solution

$$\boldsymbol{B}(\boldsymbol{x}(\boldsymbol{a}, t)\, t) = \boldsymbol{J}(\boldsymbol{x}, t)\, \boldsymbol{B}(\boldsymbol{a}, 0) \tag{4}$$

where $\boldsymbol{x}$ is the Lagrangian coordinate defined by

$$\frac{\partial \boldsymbol{x}}{\mathrm{d}t} = \boldsymbol{u}(\boldsymbol{x}, t), \quad \boldsymbol{x}(\boldsymbol{a}, 0) = \boldsymbol{a}$$

and $\boldsymbol{J}(\boldsymbol{x}, t) \equiv \partial \boldsymbol{x}/\partial \boldsymbol{a}$ is the Jacobian of the flow $\boldsymbol{u}$. For a given trajectory $\boldsymbol{x}(\boldsymbol{a}, t)$ can be calculated from the equation

$$\frac{\mathrm{d}}{\mathrm{d}t} \boldsymbol{J}(\boldsymbol{x}(\boldsymbol{a}, t), t) = \nabla \boldsymbol{u}(\boldsymbol{x}(\boldsymbol{a}, t), t) \cdot \boldsymbol{J}(\boldsymbol{x}(\boldsymbol{a}, t), t). \tag{5}$$

Then (4) says that the magnetic field $\boldsymbol{B}(\boldsymbol{x}(\boldsymbol{a}, T), T)$ can be found by following the particle $\boldsymbol{x}$ backwards in time to $t = 0$, picking up the initial condition $\boldsymbol{B}(\boldsymbol{a}, 0)$, and bringing it forward to time $t = T$ using the Jacobian of the particle path of $\boldsymbol{x}$. In order for a field vector at coordinate $\boldsymbol{x}$ to grow exponentially, $\boldsymbol{J}(\boldsymbol{x}, t)$ must have an exponentially growing eigenvalue. If, furthermore, $\boldsymbol{J}$ has an exponentially growing eigenvalue over a region of positive volume then the magnetic energy $\int |\boldsymbol{B}|^2 \, \mathrm{d}V$ will grow exponentially. As soon as $R_m < \infty$, (4) is not the solution of (1) and this observation no longer holds. Still it suggests that chaotic flows may be good candidates for fast dynamos (see Arnol'd *et al.* 1981; Bayly 1986). On the other hand $\nabla \cdot \boldsymbol{u} = 0$ implies that $\det(\boldsymbol{J}) = 1$ so that if $\boldsymbol{J}$ has an exponentially increasing eigenvalue, it must also have an exponentially decreasing one. Thus at $R_m = \infty$ the exponential stretching of magnetic field by a chaotic flow will be accompanied in general by exponential decrease in the scale of field structure. In a finite volume this effect, combined with the folding that results by necessity from stretching, produces complicated structures. Intuitively, one can then expect that for large but finite R_m extensive field dissipation will occur as fine scales are smoothed so that the growth rate of magnetic energy could be much smaller for $R_m < \infty$ than for $R_m = \infty$.

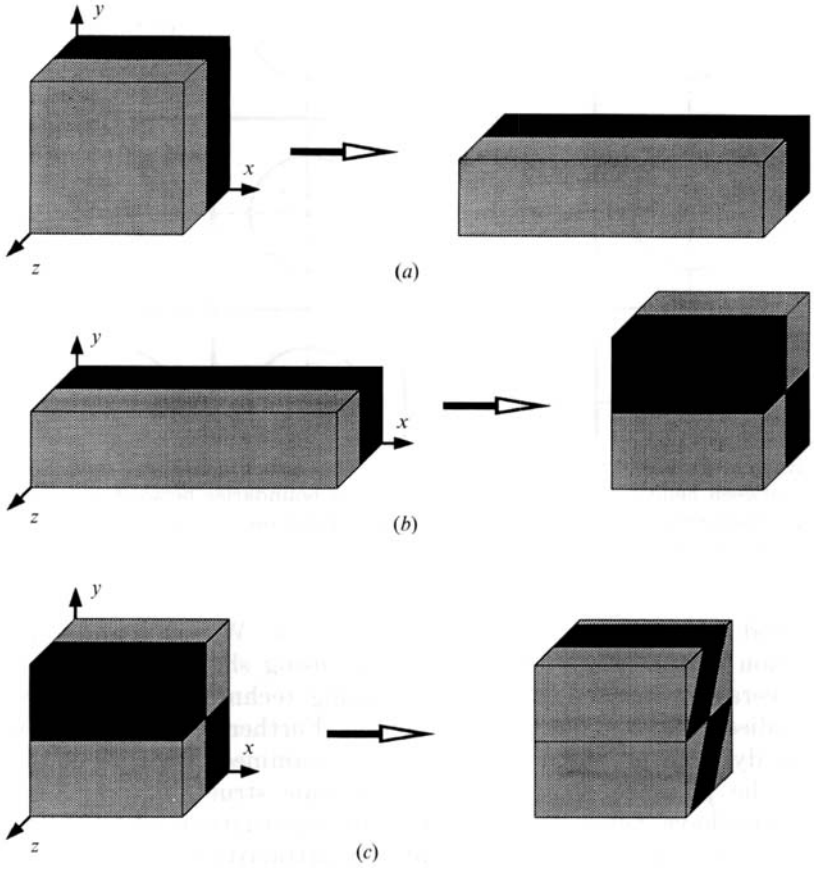

FIGURE 1. A periodic block consisting of a unit strength field in the positive x-direction (grey) and a unit strength field in the negative x-direction (black) going through the stretch–fold–shear motion. (*a*) Stretch: the cube is stretched to double its length in the x-direction and contracted to half its length in the y-direction; magnetic field strength is doubled. (*b*) Fold: the stretched cube is cut and one half is folded over the top of the other. (*c*) Shear: linear shear proportional to y is applied in the z-direction; the field in the centre of the cube points predominantly in the negative x-direction while the field on the ends points predominantly in the positive x-direction.

Thus a chaotic fast dynamo mechanism must avoid the excessive field cancellation that can result from a cascade to small scales. Also, in the spirit of fast dynamos, it is desirable that magnetic structures should occur on large scales independent of the diffusion length. Hence a fast dynamo should exhibit a sort of kinematic inverse cascade. One model with both these properties is the Bayly & Childress (1988, 1989) stretch–fold–shear map. The map, based on observations of Soward (1987), has also received the attentions of Finn *et al.* (1989, 1991). It consists of three basic motions (figure 1): a stretch that doubles field strength, a fold necessary to fit the field back into the original domain, and a shear which brings like-signed fields together and causes large-scale magnetic structures to emerge. These motions can be thought of as providing an alpha effect (together with a rotation) by pulling out and twisting magnetic field into loops.

The principal aim of this paper, then, is to present a representative time-periodic chaotic flow containing a stretch–fold–shear mechanism as a candidate for being a fast dynamo. Supporting numerical evidence will be offered using three methods: an

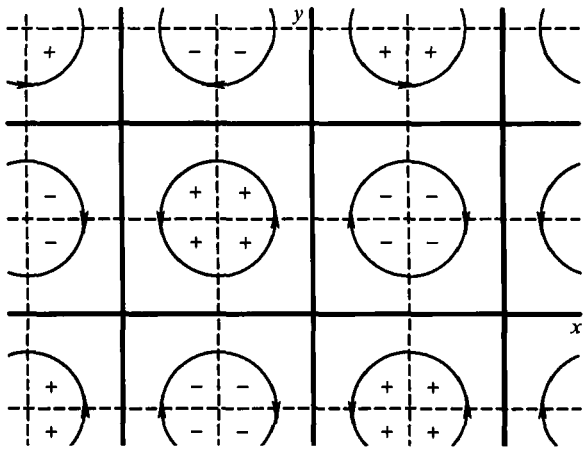

FIGURE 2. Representation of the (x, y)-plane of the unperturbed helical cell flow. Solid lines form boundaries between helical cells and dashed lines form boundaries between matched hyperbolic corners. The cells alternate between right-handed helical motion in the positive z-direction (+) and right-handed helical motion in the negative z-direction (−).

exact method using Brownian motion called the Wiener bundle method, an approximation of the Wiener bundle method using shadowing theory called the Gaussian averaging method, and an estimating technique used in previous fast dynamo studies called the flux growth method. Further, the role of diffusion in the chaotic fast dynamo process will be carefully examined. Because of the difficulty created by the presence of complicated fine-scale structure, previous studies of chaotic systems have, typically, considered special situations where diffusion can be easily handled or have made use of intuitively attractive but mathematically non-rigorous models of diffusion. A second aim of this paper, then, will be to provide some unification to the disparate viewpoints of the role of diffusion in fast dynamos.

2. The chaotic helical cell flow

The velocity field $\boldsymbol{u}$ to be tested for the fast dynamo property consists of an array of helical cells, similar to Roberts' cells (Roberts 1972), perturbed periodically in time. These helical cells are constructed by piecewise matching of two-dimensional hyperbolic corner flows at points (n, m, z) together with streamwise constant motion in the z-direction. The unperturbed velocity field is independent of z and is defined by $\boldsymbol{u}_*(x, y) = (u(x, y), v(x, y), w(x, y))$, where

$$u(x, y) = (-1)^{n+m+1}(x-n),$$

$$v(x, y) = (-1)^{n+m}(y-m),$$

$$w(x, y) = (-1)^{n+m+1}\alpha(x-n)(y-m),$$

for $n-0.5 < x \leqslant n+0.5$, $m-0.5 < y \leqslant m+0.5$, n and m integers (figure 2). One periodicity section of the motion consists of four cells. Note that this velocity field is only piecewise smooth. Calling the (x, y)-plane the horizontal one, across the matching boundaries (dashed lines in figure 2) the horizontal normal velocity is continuous but the horizontal parallel velocity is not. Thus vortex sheets are formed.

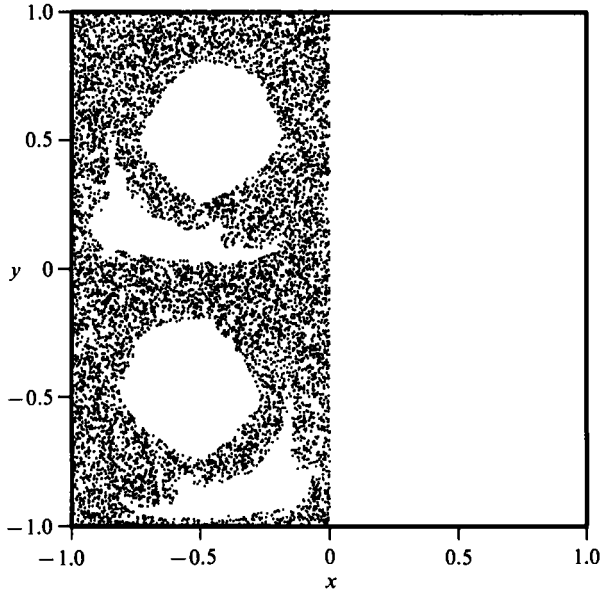

FIGURE 3. Projection onto the $z = 0$ plane of one periodicity section of the flow. 9000 particles along the unstable manifold of a hyperbolic point in a main chaotic region were released for a long period of time, filling the region. Vertical separatrices do not break so no particles cross the $x = 0$ plane.

As will soon be apparent, this form of $\boldsymbol{u}_*$ is chosen, despite the vortex sheets, for its ease of use. Effects of the discontinuities on dynamo calculations will be discussed later. Still it should be noted here that the discontinuities could be smoothed away (the Roberts' cell velocity field is an example of such a smoothing), and the author does not feel that this smoothing would have an important qualitative effect on the results. Admittedly there is no rigorous justification for this view. In certain previous studies, non-smooth velocity fields have played a critical and easily identifiable role in allowing fast dynamo action in non-chaotic flows (Soward 1987; Gilbert 1988). Here the discontinuity in the velocity field is present to facilitate computation and has no apparent direct role in assisting dynamo action. The Jacobian matrices generated by the flow may be particularly revealing in this regard – as will be demonstrated shortly, these matrices play the central role in the solution of the magnetic induction equation. In both the Soward and Gilbert fast dynamos, non-smoothness of the velocity field results in singular Jacobian matrices whereas here the Jacobian matrices will be seen to remain well-behaved despite the discontinuity in $\boldsymbol{u}$.

In order to produce chaotic regions the velocity field $\boldsymbol{u} \equiv \boldsymbol{u}_* + \boldsymbol{f}(t)$ is considered, where $\boldsymbol{f}(t) = (0, \epsilon \sin t, 0)$ for ϵ small. The perturbation breaks $y = m$ separatrices (but not $x = n$ ones) leading to a chaotic web in which some fluid particles are free to wander in the y-direction (figure 3). The open areas surrounded by the chaotic web are regions containing a mixture of regular and chaotic motion. These additional regions are presumed to be at most weakly stretching, and will not be considered. It is assumed that the region of strongest stretching and magnetic field growth is the main chaotic channel located in the area of the unperturbed separatrices.

The reasoning for considering a flow that is only piecewise smooth is apparent; the velocity field $\boldsymbol{u}$ is integrable up to the solution of a transcendental equation for the transit time through certain corners. Within a corner section of the flow the resulting

exact particle paths are given, for $n-0.5 < x_0 \leqslant n+0.5$ and $m-0.5 < y_0 \leqslant m+0.5$, by

$$x(t_0+t) = n+\bar{x}_0 \mathrm{e}^{\pm t}, \tag{6}$$

$$y(t_0+t) = m+\bar{y}_0 \mathrm{e}^{\mp t}+\tfrac{1}{2}\epsilon(\pm \sin(t+t_0)+\cos(t+t_0)), \tag{7}$$

$$z(t_0+t) = (z_0 \mp \tfrac{1}{2}\alpha\epsilon\bar{x}_0 \cos t_0) \mp \alpha\bar{x}_0(y_0-m)\,t \pm \tfrac{1}{2}\alpha\epsilon\bar{x}_0 \mathrm{e}^{\mp t}\cos(t+t_0), \tag{8}$$

where $\bar{x}_0 = x_0-n$, $\bar{y}_0 = y_0-m+0.5\epsilon(\mp \sin t_0-\cos t_0)$, and t_0 is the initial time. The top sign is used for $n+m$ odd and the bottom one for $n+m$ even. Points in corner sections with $n+m$ odd (even) will flow above the corner for $\bar{y}_0$ positive and below for $\bar{y}_0$ negative in forward (backward) time.

3. The chaotic helical flow and the standard map

It would be reassuring to check that, despite its non-smoothness, the chaotic helical cell flow is in some sense representative of a wide class of chaotic flows. This is demonstrated by relating the trajectory topology of the chaotic helical cell flow to the standard map, a canonical example (see Lichtenberg & Lieberman 1983). To do this consider a fluid particle with the (x,y)-coordinates $(0.5,y)$ at initial time t_0 for some $m-0.5 < y \leqslant m+0.5$. As the separatrices $x = 0$ and $x = 1$ are not broken by the perturbation, the particle must cross the line $x = 0.5$ again at a future time $t_0' = t_0+2T$ for some T. Using (6) and (7), at t_0' the fluid particle will have (x,y)-coordinates $(0.5,y')$, where

$$y' = m+\kappa+[-\tfrac{1}{2}\kappa+\tfrac{1}{2}\epsilon(-\sin(T+t_0)-\cos(T+t_0))]\,\mathrm{e}^{-T}+\tfrac{1}{2}\epsilon(\sin t_0'+\cos t_0'),$$

$$\kappa = \bar{y}_0/|\bar{y}_0|,$$

and T, the time required to traverse each corner, is given by the solution of the transcendental equation

$$\tfrac{1}{2} = |\bar{y}_0|\,\mathrm{e}^{T}+\tfrac{1}{2}\kappa\epsilon(-\sin(T+t_0)+\cos(T+t_0)).$$

Ignoring the z motion, the line $x = 0.5$ can be regarded as a Poincaré section. Then, as long as $\bar{y}_0 \neq 0$, the model flow can be taken as a mapping of $\bar{y}_0$ and t_0 from section to section (figure 4) given by

$$\bar{y}_0' = (-\tfrac{1}{2}\kappa+\tfrac{1}{2}\epsilon(-\sin(T+t_0)-\cos(T+t_0)))\,\mathrm{e}^{-T}+\epsilon\sin(t_0'),$$

$$t_0' = t_0+2T \pmod{2\pi},$$

where the integer part m of $\bar{y}_0$ has been removed by assuming that $\bar{y}_0$ is periodic ($\bar{y}_0 = 0.5$ is identified with $\bar{y}_0 = -0.5$). To this point all calculations are exact. Now, approximating T to first order in ϵ as $T_0 = -\ln|2\bar{y}_0|$ the map becomes

$$\bar{y}_0' = -\bar{y}_0-\epsilon|\bar{y}_0|(\cos(T_0+t_0')+\sin(T_0+t_0'))+\epsilon\sin t_0',$$

$$t_0' = t_0-2\ln|2\bar{y}_0| \pmod{2\pi}. \tag{10}$$

Assuming y_0 is in the $O(\epsilon)$ chaotic region near the old separatrices, then the quantity $\epsilon|\bar{y}_0|(\cos(T_0+t_0')+\sin(T_0+t_0'))$ is $O(\epsilon^2)$. Furthermore, as the exact map can be shown to be area-preserving, it is desirable that the approximate one be area-preserving as well in order to avoid qualitatively different properties such as sinks and sources.

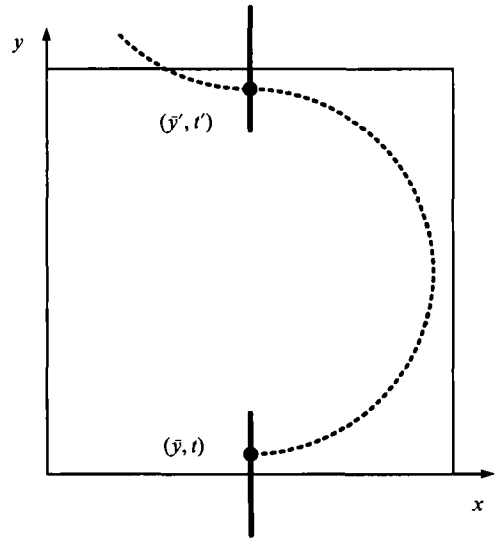

FIGURE 4. Schematic representation of the two-dimensional helical flow map. A particle path is followed as it wanders in the y-direction. Each time it passes a Poincaré section placed at $x = 0.5$, its time and $\bar{y}$ position are noted.

This can be achieved by dropping the higher-order term, a justifiable action as the approximate map is only correct to $O(\epsilon)$ anyway. Then (9), (10) become

$$\bar{y}_0' = -\bar{y}_0 + \epsilon \sin t_0'$$
$$t_0' = t_0 - 2\ln|2\bar{y}_0| \pmod{2\pi}.$$

This map is closely related to the standard map. The only important difference is that it is orientation-reversing because material points cross the Poincaré section $x = 0.5$ alternately from the left and from the right. The relation to the standard map, however, is not surprising as the standard map can typically be found in situations where separatrices are broken by time-periodic perturbations The streamline topology of the chaotic helical flow may thus also be typical of such systems. For this reason the author believes that fast dynamo results for the perturbed helical cell flow may be qualitatively similar to those for a large class of chaotic flows.

4. The flow Jacobian

In order to solve the magnetic induction equation (1) it will be necessary to calculate the Jacobians along flow trajectories. Within a section of the flow $n-0.5 < x \leqslant n+0.5$, $m-0.5 < y \leqslant m+0.5$, this is straightforward. Using (6), (7), and (8) the Jacobians are

$$\boldsymbol{J} = \begin{pmatrix} e^{\pm t} & 0 & 0 \\ 0 & e^{\mp t} & 0 \\ g & \mp\alpha\bar{x}_0 t & 1 \end{pmatrix},$$

where $g(\bar{x}_0, \bar{y}_0, t_0, t) = \mp 0.5\alpha\epsilon \cos t_0 \mp \alpha(y_0 - m)t \pm 0.5\alpha\epsilon e^{\mp t}\cos(t + t_0)$. The top sign applies for $n+m$ odd, the bottom for $n+m$ even.

However, across the matching boundaries, the streamlines have corners and hence

$\boldsymbol{J}$ is not continuous. To calculate the change in $\boldsymbol{J}$ across the boundary it is necessary to compare the action of the flow on two nearby points (x_0, y_0, z_0) and

$$(x_0+\Delta x_0, y_0+\Delta y_0, z_0+\Delta z_0)$$

as they cross from one corner region to another. Then by constructing the quantities $\Delta\zeta/\Delta\zeta_0$, $\zeta = x, y, z, \zeta_0 = x_0, y_0, z_0$, and taking the limit $\Delta x_0, \Delta y_0, \Delta z_0 \to 0$ it is possible to calculate the jump Jacobians

$$\boldsymbol{J}_1 = \begin{pmatrix} 1 & 0 & 0 \\ \mp 4(y-m) & 1 & 0 \\ 0 & 0 & 1 \end{pmatrix},$$

$$\boldsymbol{J}_2 = \begin{pmatrix} 1 & \mp 4\dfrac{x-n}{1-2\epsilon\sin t} & 0 \\ 0 & 1 & 0 \\ 0 & 0 & 1 \end{pmatrix}$$

for trajectories crossing into corner regions with $n+m$ odd and $n+m$ even respectively. These shear matrices result from the corners formed on the streamlines crossing these discontinuities. The top and bottom signs are for trajectories moving in the negative and positive x-directions respectively in the case of $\boldsymbol{J}_1$, and for trajectories moving in the negative and positive y-directions respectively in the case of $\boldsymbol{J}_2$.

5. The dynamo mechanism

An interesting property of the perturbed cellular flow in particular and of many three-dimensional flows with broken separatrices in general is that they contain an easily identifiable mechanism for fast dynamo action, namely the stretch–fold–shear mechanism. To see this, consider the hyperbolic fixed points (n, m) of the unperturbed flow. These become hyperbolic periodic points

$$(n, m+0.5\epsilon[\pm\sin(t+t_0)+\cos(t+t_0)])$$

after adding the perturbation. The periodic points with $n+m$ odd are out of phase with the ones with $n+m$ even. Fluid particles leaving periodic points with $n+m$ odd will in general no longer asymptote to periodic points with $n+m$ even. Thus the old horizontal separatrices are broken and a stretch–fold action results from broken separatrices folding up against hyperbolic points in the (x, y)-plane (shown schematically in figure 5), well-known events in chaotic systems. Shearing is provided by the differential velocity in the z-direction. This kind of stretching and folding is closely associated with transverse homoclinic and heteroclinic points and thus with chaos (see e.g. Guckenheimer & Holmes 1983).

The stretch–fold–shear map and the chaotic helical cell flow themselves are exceptional time-dependent chaotic systems in that they have a Liapunov exponent equal to zero (corresponding to a Liapunov vector pointing in the z-direction in both cases). The reasons for this degeneracy are to allow the problem to be reduced to two dimensions and to make the dynamo mechanism more understandable. A zero Liapunov exponent is not necessary for the stretch–fold–shear mechanism, however. All that is needed are a principal stretching direction, a principal contracting direction, and a third direction in which shearing occurs.

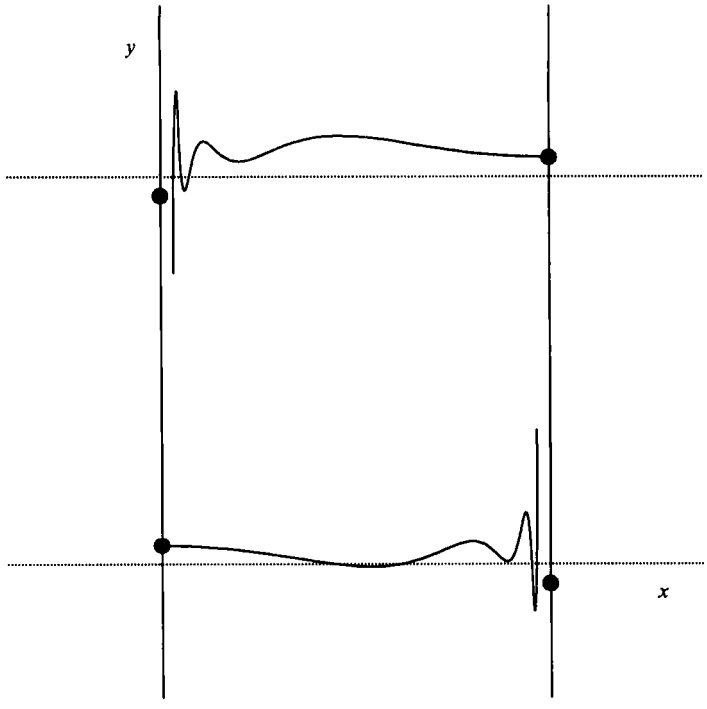

FIGURE 5. Schematic projection of the unstable manifolds of four hyperbolic points in the (x, y)-plane. Solid lines are unstable manifolds of the perturbed flow, dotted lines are horizontal separatrices of the unperturbed flow that are broken by the perturbation.

6. Solving the induction equation

As previously mentioned, when $R_m = \infty$ the magnetic induction equation (1) can be reduced to ODE's by the Cauchy solution. The Cauchy solution no longer holds when $R_m < \infty$. However, using Brownian motion theory, it is still possible to reduce equation (1) to the solution of ODE's. The method involves averaging the Cauchy solution over a set of noisy orbits called a Wiener bundle. This method has been made use of by Chorin (1973), Kraichnan (1976), and Drummond, Duane & Horgan (1984) in turbulence studies, and more recently has been suggested for fast dynamos (Molchanov, Ruzmaikin & Sokolov 1985; Gilbert & Childress 1990). The Wiener bundle is made up of Wiener trajectories defined by

$$\mathrm{d}\boldsymbol{x} = \boldsymbol{u}\,\mathrm{d}t + \sqrt{2}\,R_m^{-\frac{1}{2}}\mathrm{d}\boldsymbol{w}, \tag{11}$$

where $\boldsymbol{w}(t)$ is a (Gaussian) random process with independent increments (see e.g. McKean 1969) such that

$$\langle w_i(t)\rangle = 0, \quad \langle w_i(t)\, w_j(t)\rangle = \delta_{ij}\, t. \tag{12}$$

The Wiener bundle solution to (1) is given by

$$\boldsymbol{B}(\boldsymbol{x}, t) = \langle \boldsymbol{J}(\boldsymbol{x}, \boldsymbol{a}_0, \boldsymbol{X}, t)\, \boldsymbol{B}(\boldsymbol{a}_0, 0)\rangle, \tag{13}$$

where the average is over all Wiener trajectories $\boldsymbol{X}(s)$ starting at a random point $\boldsymbol{X}(0) = \boldsymbol{a}_0$ and ending at a given (non-random) point $\boldsymbol{X}(t) = \boldsymbol{x}$. Note the close relation to the Green's function solution; the solution is calculated pointwise by adding the contributions from each possible initial point. See also Vishik (1989) for the use of Green's function techniques in fast dynamo studies.

The Weiner bundle solution differs from the Cauchy solution in that it averages the contribution from many arriving particles rather than only one. $\boldsymbol{J}$ is calculated as before using (5). Note however the subtle point that the Jacobian $\boldsymbol{J}$ is calculated using the velocity field $\boldsymbol{u}$ without noise but over the path of the noisy Wiener trajectory. In this way the Wiener bundle solution 'unfreezes' the magnetic field by allowing field vector slippage but does not introduce additional stretching. For a rigorous proof of (13) see e.g. McKean (1969). However, to verify it non-rigorously expand $\boldsymbol{B}(\boldsymbol{x}, t+\Delta t)$ and retain the necessary low-order terms to get

$$
\begin{aligned}
B(\boldsymbol{x}, t+\Delta t)_i &= \langle J(\boldsymbol{x}, \boldsymbol{a}_t, \boldsymbol{X}, \Delta t)_{ij} B(\boldsymbol{a}_t, t)_j \rangle \\
&\approx \langle J(\boldsymbol{x}, \boldsymbol{x}, \boldsymbol{X}, 0))_{ij} B(\boldsymbol{x}, t)_j \rangle + \left\langle J(\boldsymbol{x}, \boldsymbol{x}, \boldsymbol{X}, 0)_{ij} \frac{\partial B_j}{\partial x_k} (\boldsymbol{a}_t - \boldsymbol{x})_k \right\rangle \\
&\quad + \left\langle \frac{\partial J_{ij}}{\partial t} B(\boldsymbol{x}, t)_j \Delta t \right\rangle + \left\langle \tfrac{1}{2} J(\boldsymbol{x}, \boldsymbol{x}, 0)_{ij} \frac{\partial^2 B_j}{\partial x_k \partial x_l} (\boldsymbol{a}_t - \boldsymbol{x})_k (\boldsymbol{a}_t - \boldsymbol{x})_l \right\rangle \\
&= \langle \boldsymbol{B}(\boldsymbol{x}, t)_i \rangle - \left\langle \frac{\partial B_i}{\partial x_j} (\boldsymbol{u} \Delta t + \sqrt{2} R_{\mathrm{m}}^{-\frac{1}{2}} \boldsymbol{w}(\Delta t))_j \right\rangle + \left\langle \left(\frac{\partial \boldsymbol{u}_i}{\partial x_j} \cdot J_{jk} \right) \boldsymbol{B}(\boldsymbol{x}, t)_k \Delta t \right\rangle \\
&\quad + \left\langle \tfrac{1}{2} \frac{\partial^2}{\partial x_j} \frac{B_i}{\partial x_k} (\boldsymbol{u} \Delta t + \sqrt{2} R_{\mathrm{m}}^{-\frac{1}{2}} \boldsymbol{w}(\Delta t))_j (\boldsymbol{u} \Delta t + \sqrt{2} R_{\mathrm{m}}^{-\frac{1}{2}} \boldsymbol{w}(\Delta t))_k \right\rangle \\
&= B(\boldsymbol{x}, t)_i - (\boldsymbol{u} \cdot \nabla \boldsymbol{B})_i \Delta t + (\boldsymbol{B} \cdot \nabla \boldsymbol{u})_i \Delta t + (R_{\mathrm{m}}^{-1} \nabla^2 B)_i \Delta t.
\end{aligned}
$$

Spatial derivatives of $\boldsymbol{J}$ are not included because of the slippage property mentioned above.

7. Numerical methods

The primary method to be used for calculations will be the Wiener bundle solution described in the previous section. The method is well suited for several reasons. Firstly, as already mentioned, it reduces the problem to the integration of ODE's. In particular, for the chaotic helical cell flow these ODE's can be piecewise integrated, further reducing the problem to that of map iteration. Secondly, although the method requires that the magnetic field be calculated for each point separately, the value of the field at a single point is all that is necessary in order to calculate the field growth rate. Thirdly, the method allows study of higher magnetic Reynolds numbers than would otherwise be possible, as will be seen shortly. Fourthly, an explicit error estimation can be made.

The Wiener bundle solution is also of interest because for small magnetic diffusivity (or large magnetic Reynolds number) it provides some insight into the smoothing role that diffusion plays in the fast dynamo process. To see this, regard the Wiener bundle as a cloud of noisy orbits, released from a point $\boldsymbol{p}$, which travel backwards in time. As the noise causes them to spread, the chaotic flow pulls the cloud into a long thin ($O(R_{\mathrm{m}}^{-\frac{1}{2}})$) sausage (Gilbert 1990, personal communication) along the stable manifold of the preimages of $\boldsymbol{p}$ (in backwards time the stable manifold is stretched exponentially). This suggests that the Wiener bundle solution for large R_{m} can be well approximated by an average of the Cauchy solution over the stable manifold of $\boldsymbol{p}$. Noisy Wiener trajectories are approximated by nearby exact trajectories through the use of the shadowing principle.

Shadowing can be defined as follows (Newhouse 1980). Let $\boldsymbol{f}$ be a chaotic map (such as the time-one integration of a chaotic flow) and let $\{\boldsymbol{y}_i\}$, $-n \leqslant i \leqslant 0$, be a noisy

Wiener trajectory of f. The trajectory $\{y_i\}$ is said to be an ϵ pseudo-orbit of f if $|f(y_i)-y_{i+1}| < \epsilon$, $-n \leqslant i < 0$. An exact trajectory $\{x_i\}$, $-n \leqslant i \leqslant 0$, of f is said to δ shadow $\{y_i\}$ if $|x_i-y_i| < \delta$, $-n \leqslant i \leqslant 0$. The map f has the shadowing property if given any $\epsilon > 0$ small enough there exists a δ such that any ϵ pseudo-orbit can be δ shadowed by an exact one. That is, there is an exact trajectory near to any slightly noisy one. Note that n could be ∞ and that δ depends only on ϵ and not on n. An example of a map with the shadowing property is a uniformly hyperbolic system like the Arnol'd cat map (Arnol'd & Avez 1968).

The above situation occurs when a bundle of Wiener trajectories at small diffusivity is considered in a map with the shadowing property. For although the noise on a Wiener trajectory is Gaussian and hence not necessarily small, for asymptotically small diffusivity and finite time the probability of a given trajectory ever being perturbed at a noise level larger than any fixed ϵ goes to 0. Hence for small enough diffusion a given Wiener trajectory in a system with the shadowing property can with arbitrarily high certainty be shadowed arbitrarily accurately over finite times. In Klapper (1992) it is shown in the case of scalar advection that for asymptotically small diffusivity the Wiener bundle can be well approximated by a bundle of exact shadowing trajectories along the stable direction of $\boldsymbol{p}$ with Gaussian density where the variance σ^2 is given by

$$\sigma^2 = 2R_{\mathrm{m}}^{-1} \sum_{j=0}^{\infty} \lambda_{(-j)}^{2j}. \tag{14}$$

$\lambda_{(-j)}$ is the contracting factor of f along the stable manifold of $f^{-j}(\boldsymbol{p})$. See the Appendix for the extension to vectors. Thus the Wiener bundle solution can be approximated asymptotically by the average of the Cauchy solution along the stable manifold of $\boldsymbol{p}$ against the above Gaussian distribution for finite times at least. This method of approximating the exact solution (13) will henceforth be called the Gaussian averaging method. Since the stable direction is approximately the direction of small scales then for systems with the shadowing property diffusion has the effect of smoothing structure built up in the Cauchy solution over the lengthscale σ (which is independent of time).

This paper is a numerical study of fast dynamo action and hence is concerned with finite times. From a theoretical point of view, definition (2) implicitly contains a double limit with $t \to \infty$ followed by $R_{\mathrm{m}} \to \infty$. Because of the singular nature of sending R_{m} to infinity, the two limiting processes do not in general commute and thus the order of the double limit is crucial. For fixed time, $\boldsymbol{B}$ reduces trivially to the Cauchy solution when $R_{\mathrm{m}} \to \infty$. Thus in order that the Gaussian averaging method be a useful analytical tool it is important that it should still make sense for infinite time at fixed magnetic Reynolds number. The difficulty with this extension is that over infinite time any given Wiener trajectory will, with probability one, experience large noise events and hence will not be shadowable. This is only to be expected as for very long times there must be at least the chance for diffusion to have long-range effects. This large noise problem can be overcome in a wide class of hyperbolic systems by approximating Wiener trajectories with *almost* shadowing exact trajectories, that is, trajectories that shadow for almost all of the time (Klapper 1991). For the purposes of this paper, it is enough to note that, given the range of R_{m} used, the times considered here, although finite, are on the one hand long enough for the Cauchy solution to develop small scales well below the diffusion length and on the other hand not so long that large noise events are likely. Thus it is expected

that the Gaussian averaging results reported give an accurate and non-trivial picture of local diffusivity effects.

The Gaussian averaging method depends on the shadowing principle which does not hold for non-hyperbolic systems like the chaotic helical cell flow. However, numerical work of Grebogi *et al.* (1990) has produced evidence that shadowing is usually possible for long times in typical non-hyperbolic volume-preserving chaotic systems, and hence the method might be expected to provide a good approximation to the exact solution. Furthermore, when shadowing does break down, it does so for trajectories that pass through weakly stretched areas. Previous fast dynamo studies have indicated that averages of the Cauchy solution are dominated by the contributions of a relatively small number of strongly stretched trajectories (Finn & Ott 1988; Finn *et al.* 1991). So those trajectories for which shadowing breaks down may be unimportant in the final average.

Thus, as long as the effects of shadowing breakdown are unimportant, diffusion may be thought of as Gaussian smoothing of small scales developed by the Cauchy solution. This is in agreement with an idea put forward previously by Finn & Ott (1988). They postulated that fast dynamo growth rates in chaotic systems can be measured by computing the flux growth rate $(1/T)\ln|\int \boldsymbol{B}\,\mathrm{d}\boldsymbol{x}|$ of the Cauchy solution in a neighbourhood of a point $\boldsymbol{p}$. That is, they suggested that the growth rate of a chaotic dynamo at $R_\mathrm{m} = \infty$ could be found by averaging the Cauchy solution in a small region against a uniform distribution. This method for calculating the dynamo growth rate will henceforth be called the flux growth method. Averaging over a small region should give the same answer as averaging only over the stable direction since the Cauchy solution is approximately constant in the strongly stretched unstable directions. Furthermore, when calculating exponential growth rates in chaotic systems it can be expected that, typically, averaging against a Gaussian density and averaging against a uniform density will give the same answer. Thus the two methods seem likely to agree and in fact the Gaussian averaging method then provides some verification for the flux growth method. However, it seems that in the same way as the variance (14) depends on R_m, a finite R_m is implicitly assumed in the flux growth method when the size of averaging region is chosen. Thus the growth rate calculated by the flux growth method may correspond more closely to a large but finite R_m than to $R_\mathrm{m} = \infty$. Another way of saying this is that by averaging over a box of size l, field structures of size smaller than l are smoothed away. Also implicitly assumed by both the Gaussian averaging and flux growth methods is that the role of diffusion is limited to the smoothing of small scales. This bears dangerous similarities to preassuming fast dynamo action. Evidence shown here and other places (Bayly & Childress 1988; Finn & Ott 1990) supports the idea for chaotic systems; nevertheless it is an assumption that should be treated with some care. The theory of Gaussian averaging may provide a clue to understanding when the role of diffusion becomes non-local. The method breaks down when shadowing does. Hence, as previously mentioned, noisy orbits that cannot be shadowed are of interest as they may indicate what non-local effects diffusion can have.

As a further note, the fact that the averaging is done over a finite line segment for finite R_m agrees with Finn & Ott's proposal that the appropriate upper bound on field growth in a two-dimensional chaotic system is not the growth rate of an infinitesimal line segment (i.e. the largest Liapunov exponent) but the growth rate of a finite line segment, which they identify with the topological entropy. (The growth rate of a finite line segment is greater than or equal to that of an infinitesimal line segment, but otherwise the two are in general unrelated.) In fact, a slight generalization to

three dimensions is possible. In this case the Gaussian averaging method requires that the integration be taken over the stable manifold which again, for a volume-preserving system, suggests that topological entropy gives an upper bound to the growth rate (for a three-dimensional volume-preserving chaotic system, the topological entropy can be identified with the largest growth rate of lines and surfaces, see Yomdim 1987, Newhouse 1986), although the growth rate of finite line segments is still the best bound.

8. Numerical results

The growth rate of the magnetic field in the chaotic helical cell flow $\boldsymbol{u}$ was studied using the three methods described in the previous section. For the exact Wiener bundle solution the flow was alternated with pulses of diffusion, a technique suggested by Backus (1958) that has been used in several previous fast dynamo studies (e.g. Bayly & Childress 1988). With this method, fast periods of fluid flow without diffusion are alternated with periods of fluid stasis in which diffusion is allowed to act long enough to smooth fine-scaled magnetic structure. The principal reason for separating advection and diffusion here is to avoid technical difficulties associated with Wiener trajectories crossing and recrossing matching boundaries. It is, however, not strictly necessary to use this device.

Further simplification is possible due to the choice of velocity field $\boldsymbol{u}$. It has the significant advantage that it allows solutions of the form $\boldsymbol{B} = \boldsymbol{b}(\boldsymbol{x}_{\mathrm{H}}, t)\,\mathrm{e}^{2\pi \mathrm{i} k z}$, where $\boldsymbol{x}_{\mathrm{H}} = (x, y)$. In this case the z-component of diffusion separates out and has the sole effect of reducing the field by a factor $\exp[-(4\pi^2 k^2/R_{\mathrm{m}})T]$ at each diffusion pulse, where T is the length of the pulse. This factor is included in the calculations (although with the parameters used it has no noticeable effect) and the problem is reduced to two dimensions.

For the purpose of this study the perturbation parameter has been set to $\epsilon = 0.1$. Varying ϵ at fixed R_{m} would be interesting as well. Presumably a transition from the chaotic dynamo mechanism to the Roberts' cell dynamo mechanism observed by Soward (1987) would occur when the sizes of the chaotic layer and diffusive boundary layers become comparable. Such a study lies beyond the scope of this paper, however.

Figure 6 shows the growth rate of the magnetic field $\boldsymbol{B}$ at the point

$$\boldsymbol{p} = (-0.5,\ -0.005,\ 0)$$

versus time for several magnetic Reynolds numbers. Results for other points in the chaotic region were consistent. In all cases the initial magnetic field is $\boldsymbol{B}_0 = (\mathrm{e}^{3.5\pi \mathrm{i} z}, 0, 0)$ and shear parameter is $\alpha = 2$. The calculations were done using the exact Wiener bundle method averaging over an ensemble of approximately 3×10^6 particles for each R_{m} (except for $R_{\mathrm{m}} = 10^6$ where 6×10^6 particles were used). The magnetic field at $\boldsymbol{p}$ was calculated for increasing flow times but constant phase of 2.28. That is, the field was calculated for a series of different flows, each starting one time unit earlier than the previous one but each stopping at $t = 2.28$. The times shown in figure 6 are the time lengths of these flows. The reason for doing this is to factor out the natural 2π frequency of the periodic perturbation by always finishing at the same phase, thus making it easier to see the underlying growth rate. In order to estimate errors the bundle was divided into sets of 100 noisy trajectories. Each set was then treated as a Gaussian variable, allowing a sample standard deviation to be calculated. Error bars, not included in figure 6, are small except for the last few points where they grow

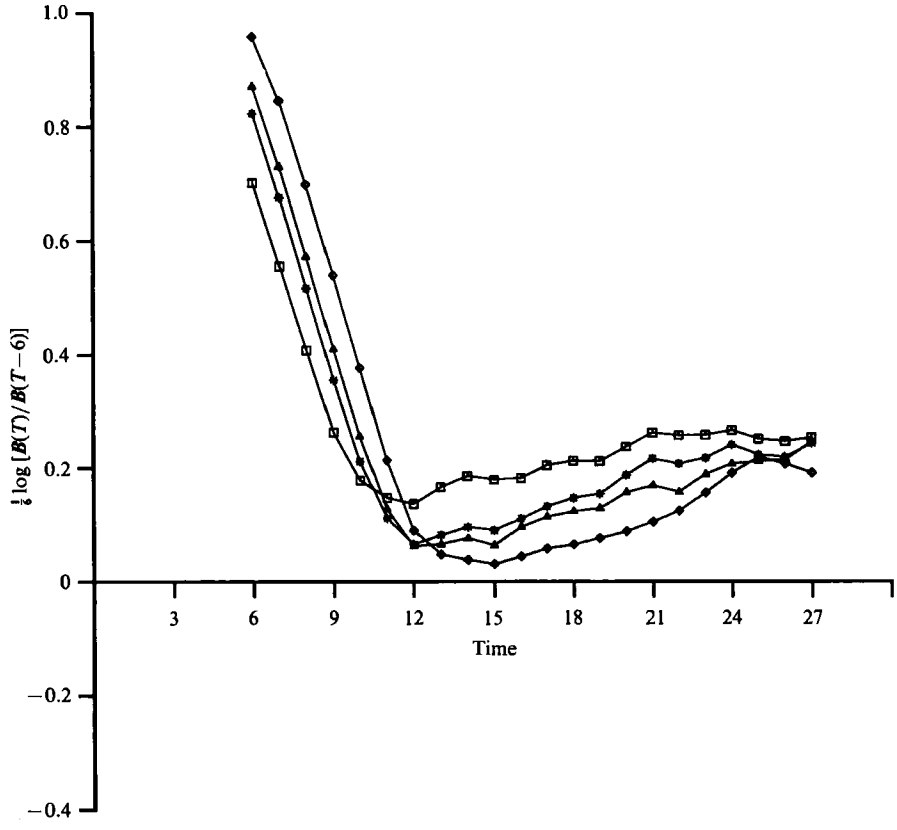

FIGURE 6. Growth rates of the magnetic field $\boldsymbol{B}_0 = (e^{3.5\pi iz}, 0, 0)$ at the point $\boldsymbol{p} = (-0.5, -0.005, 0)$ for $R_m = 2\times10^4$ (□), $R_m = 10^5$ (*), $R_m = 2\times10^5$ (△), and $R_m = 10^6$ (◇). The shear parameter is set at $\alpha = 2$.

(exponentially) to the level of approximately ± 0.02 (except for the curve $R_m = 10^6$ for which the error bars are approximately twice as large). The growth rate of uncancelled field, that is, the growth rate of $\int |\boldsymbol{B}|$ integrated over the Wiener bundle, settles to approximately 0.32, corresponding to a doubling time of about 2.2 time units. This growth rate is considerably larger than the magnetic field growth rate. Thus most of the magnetic field is cancelling and as time increases $|\int \boldsymbol{B}| / \int |\boldsymbol{B}|$ is an exponentially small quantity. Hence exponentially increasing resolution is required in time, severely limiting the total allowable evolution time.

The results suggest that once enough time has passed so that the cloud of noisy Wiener trajectories is well mixed throughout the chaotic region the growth rate becomes independent of R_m. The cloud will take a much longer time ($t \sim R_m$) to spread to the island regions. However, contributions from the islands are expected to be small because of flux expulsion and weak stretching. To get an idea of the time T needed for the cloud to mix throughout the chaotic region note that equation (14) suggests that the Wiener bundle can be approximated by a line of particles through $\boldsymbol{p}$ of length proportional to $(2R_m^{-1}\sum \lambda_{(-j)}^{2j})^{\frac{1}{2}}$. As finite lines grow at a rate $e^{\lambda_L t}$ where $\lambda_l > 0$ is the topological entropy, then the time T for the Wiener bundle to be stretched to a sausage of length l is approximately

$$T = \frac{1}{2\lambda_L} \ln\left(\frac{l^2 R_m}{2\sum \lambda_{(-j)}^{2j}}\right). \tag{15}$$

Thus the time depends on ln R_m, in qualitative agreement with figure 6. It is this feature that counterbalances the fact that exponentially more points in time are needed to resolve the Wiener bundle solution, thus allowing the Wiener bundle method to be a useful technique for large magnetic Reynolds numbers. Figure 7 shows, at various times, one spatial periodicity section of the flow containing 8000 Wiener trajectories originating from the point $\boldsymbol{p}$ at $R_m = 10^5$. Figure 8 shows the same for $R_m = 10^6$. The positions of the trajectories are projected onto the plane $z = 0$. In the final frame of each figure the Wiener cloud is well mixed through the chaotic regions on both sides of the invariant separatrix $x = 0$, indicating that the field near $\boldsymbol{p}$ at least may have settled down to an eigenfunction.

In figure 9 the growth rates calculated using all three methods are shown at $R_m = 10^5$ and 10^6. The variances of the Gaussian and uniform distributions were chosen using (14). In the case $R_m = 10^5$ the three curves agree well until approximately $T = 12$. At that time a large number of Wiener trajectories enter an area of weak stretching (see figure 7*a*) indicating that the shadowing assumption may begin to break down at this diffusivity. Also many trajectories have jumped across the plane $x = 0$. However, the Gaussian method still gives fair agreement with the Wiener bundle method for later times. The flux growth method seems to require greater resolution, and the accuracy of that curve is suspect after $t = 21$. In the case $R_m = 10^6$ the results are similar but agreement is for somewhat longer times as might be expected from the larger magnetic Reynolds number.

In figure 10, the relative error $|\boldsymbol{B}_G(\boldsymbol{p},t) - \boldsymbol{B}(\boldsymbol{p},t)|/|\boldsymbol{B}(\boldsymbol{p},t)|$ is plotted for $R_m = 10^5$ and, where $\boldsymbol{B}_G(\boldsymbol{p},t)$ is the value of the magnetic field at $\boldsymbol{p}$ at time t calculated using the Gaussian method, and $\boldsymbol{B}(\boldsymbol{p},t)$ is the same using the Wiener bundle method. Excellent quantitative agreement is seen for early times despite strong dependence of both methods on the level of diffusivity. Furthermore although the two vectors are growing exponentially, they continue to remain within the same order of each other for later times. In figures 11 and 12, a short line segment centred at the point $\boldsymbol{p}$ was released and was allowed to advect backwards in time. The projection of the resulting line segment was then plotted. In figure 11 the length of the initial line segment was chosen to be four times the standard deviation used in the Gaussian method for $R_m = 10^5$, while the length of the initial line segment used for figure 12 was chosen similarly except with $R_m = 10^6$. Comparing figures 11 and 12 with figures 7 and 8 gives an indication of why the Gaussian averaging method approximates well the Wiener bundle method; the line segments in figures 11 and 12 are good representations of those parts of the clouds in figures 7 and 8 that do not cross a separatrix. As mentioned above the discrepancies between the Gaussian and Wiener bundle methods seen in figures 9 and 10 may be a result of Wiener trajectories that cannot be shadowed, such as those which cross separatrices. Because of flow symmetry and since initial magnetic fields used here are independent of x and y, differences in growth rate are not expected to remain significant over long times.

9. Conclusions

A helical cell flow has been studied for fast dynamo action. The flow contains an easily identifiable stretch–fold–shear mechanism arising from the occurrence of transverse heteroclinic points, a common feature of chaotic flows. The principal numerical method used, the Wiener bundle averaging technique, treats diffusion exactly at the expense of limiting evolution time. However, larger magnetic Reynolds numbers can be investigated than would have been possible using the

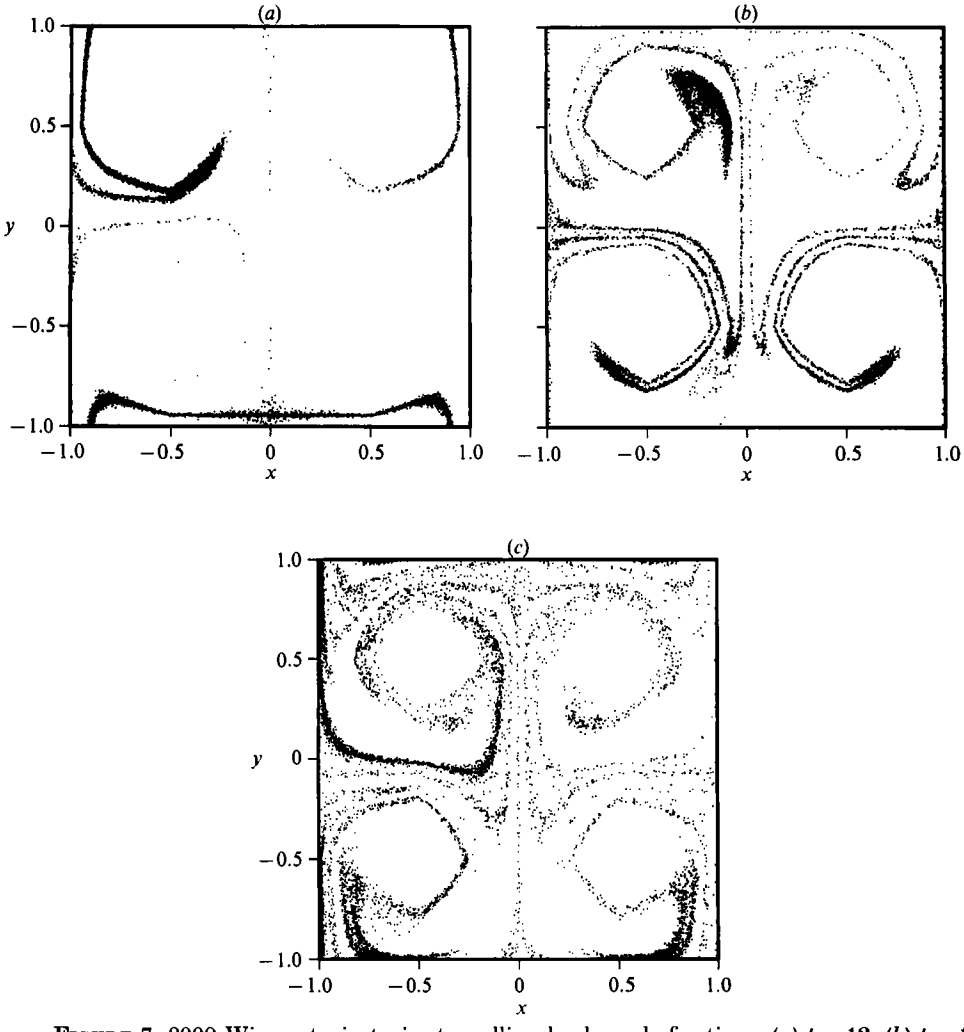

FIGURE 7. 8000 Wiener trajectories travelling backwards for times (*a*) $t = 12$, (*b*) $t = 17$, and (*c*) $t = 22$ from the point $\boldsymbol{p} = (0.5, -0.005, 0)$ at $R_m = 10^5$.

available resources with a finite difference or spectral method such as those used in some previous studies of unsteady flows (Bayly & Childress 1988; Otani 1988). Clear evidence of dynamo action was observed over a range of magnetic Reynolds numbers. Furthermore, after an initial period during which fine-scale structure was created, the magnetic field growth rate appeared to become independent of magnetic Reynolds number, suggests fast dynamo action.

In order to better understand the diffusion process the Gaussian averaging method was introduced. The method, an approximation to the Wiener bundle average, is based on the approximation of noisy Wiener trajectories by exact ones through the use of the shadowing principle. It has the advantage of reducing the problem to the dimension of the stable manifold, which is one in the case of the chaotic helical cell flow. The Gaussian averaging method also offers insight into the role that diffusion plays in the smoothing of fine scales, supporting the idea that diffusion has no direct effect in the chaotic fast dynamo mechanism. Comparisons of the results from the exact Wiener bundle method and the approximate Gaussian average method showed

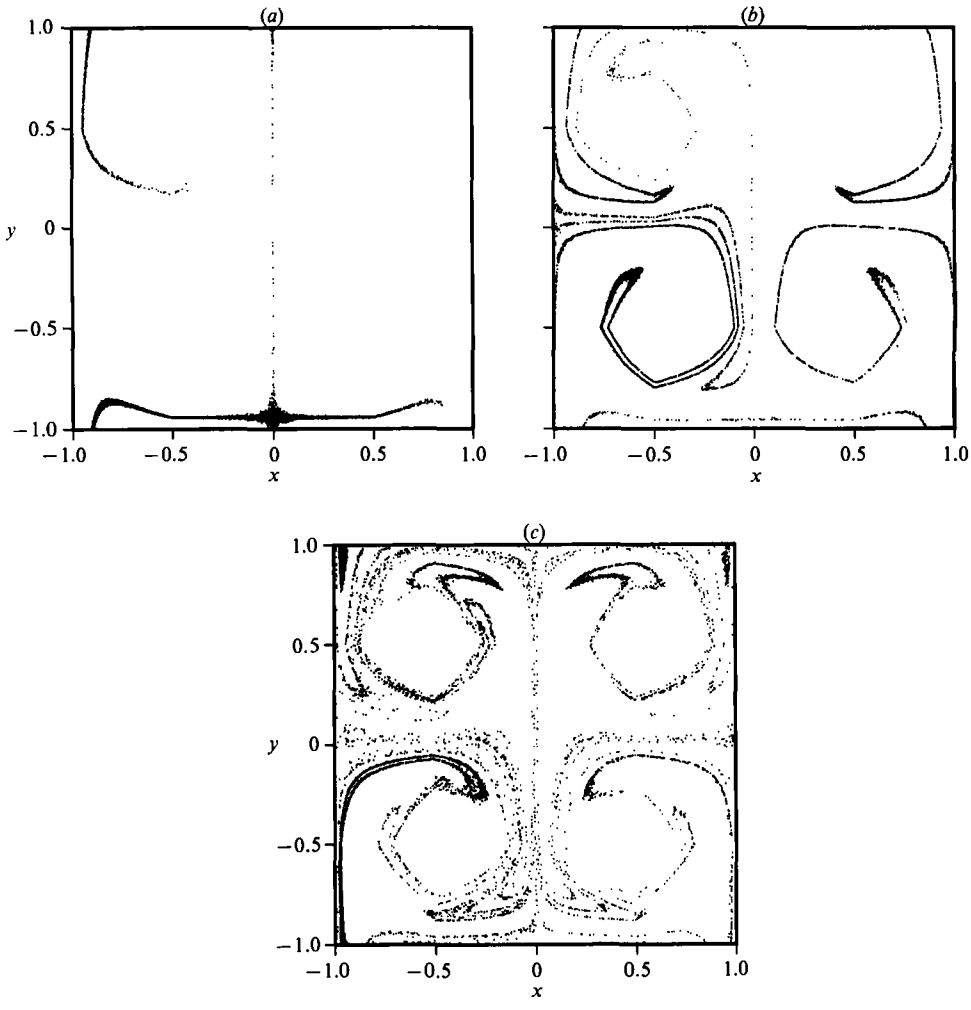

FIGURE 8. 8000 Wiener trajectories travelling backwards for times (*a*) $t = 12$, (*b*) $t = 18$, and (*c*) $t = 24$ from the point $\boldsymbol{p} = (-0.5, -0.005, 0)$ at $R_m = 10^6$.

good quantitative agreement for moderate times despite the sensitivity of both methods to magnetic Reynolds number at early times. It is expected that quantitative agreement would continue to improve as R_m is increased.

Evidence has been presented suggesting that growth rates become independent of magnetic Reynolds number after short times and that diffusion has only the passive role of the smoothing of the fine-scale field created by chaotic stretching and folding. These are indicators of fast dynamo action. However, as there are known examples of flows in which growth rates decay extremely slowly with increasing magnetic Reynolds number, it will always be desirable to obtain analytic results. Without resorting to artifice, such results for chaotic systems like the chaotic helical cell flow seem difficult.

The author is deeply indebted to Steve Childress and Andrew Gilbert for many hours of patient assistance. He would also like to thank Andrew Soward and Mike

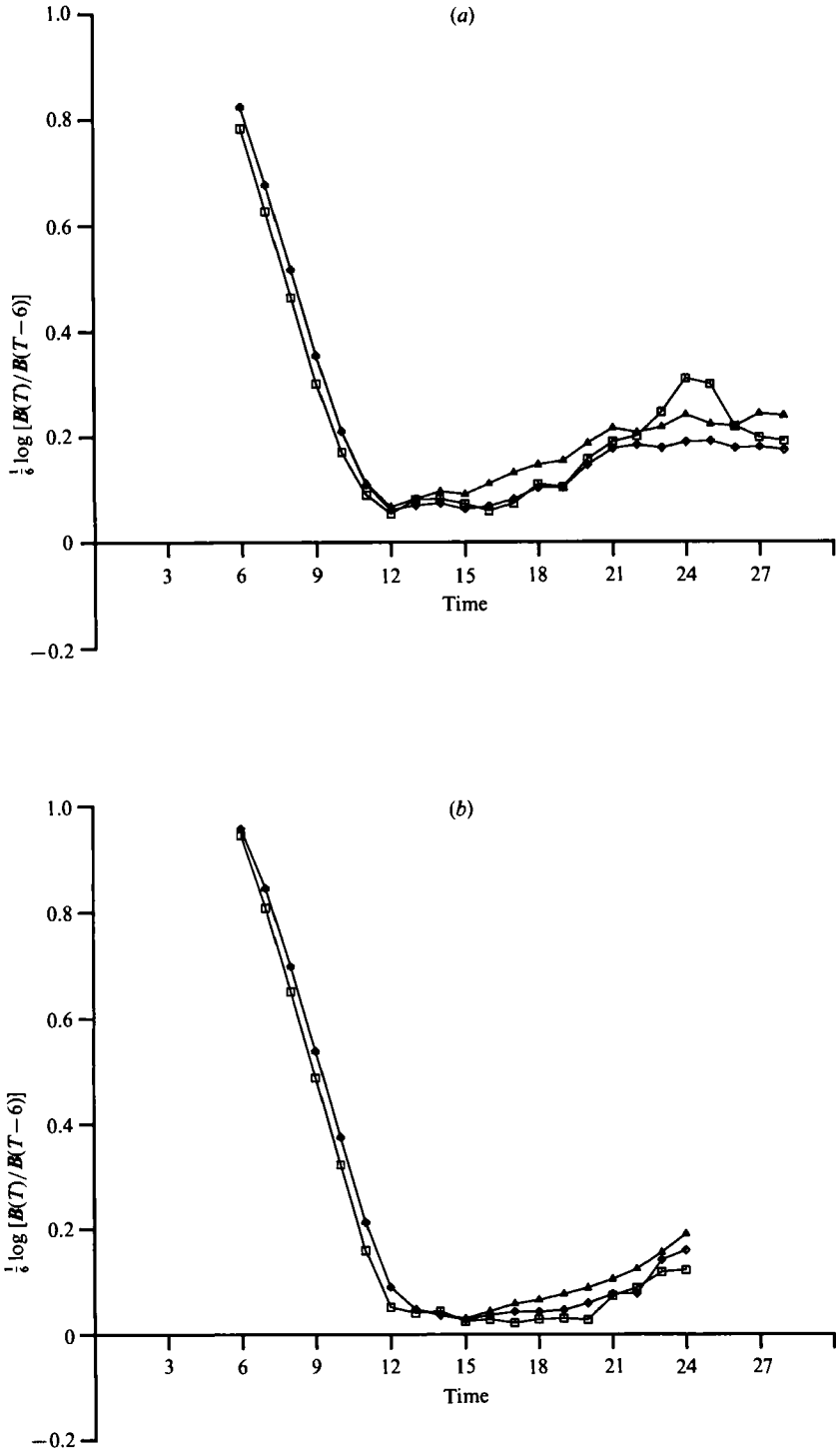

FIGURE 9. Comparison of the magnetic field growth rate at the point $\boldsymbol{p} = (-0.5, -0.005, 0)$ calculated at (*a*) $R_m = 10^5$ and (*b*) $R_m = 10^6$ using the Wiener bundle method (△), the Gaussian averaging method (◇), and the flux growth method (□).

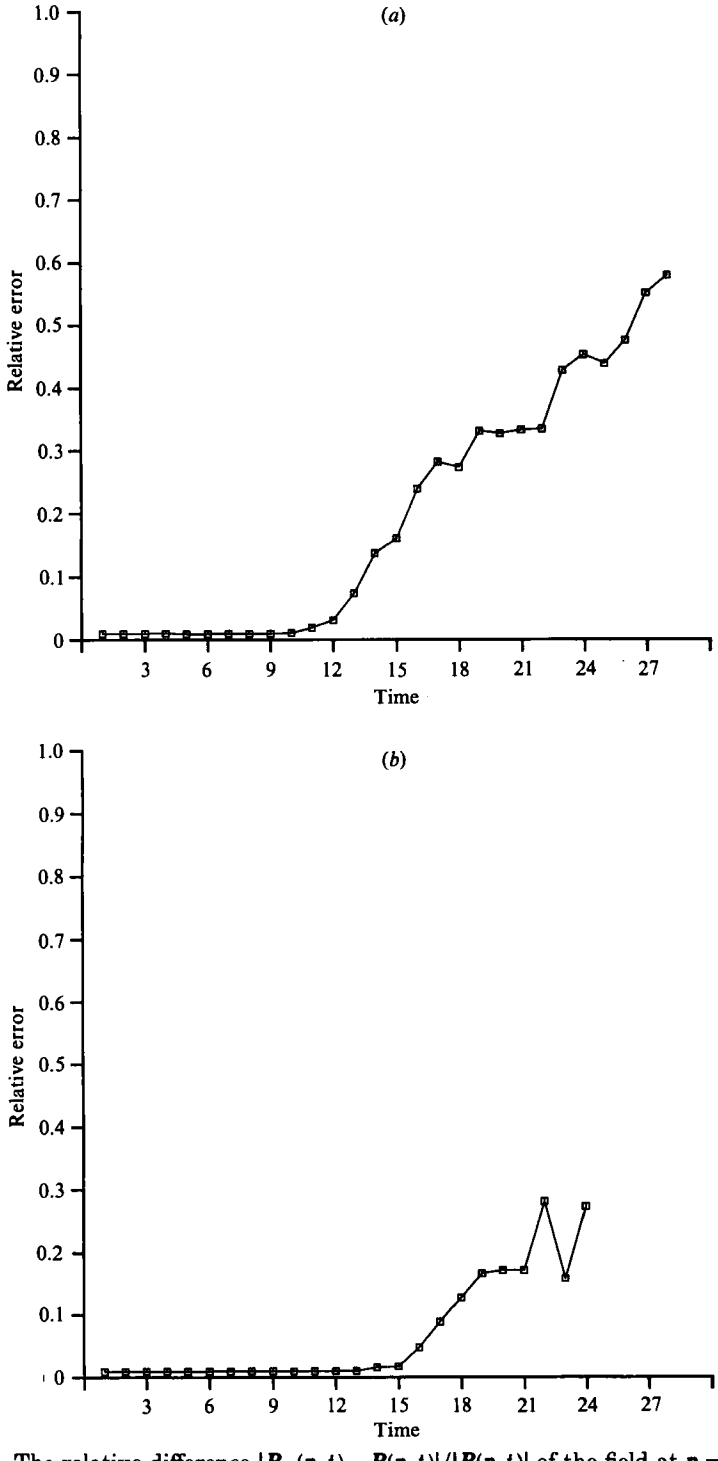

FIGURE 10. The relative difference $|\boldsymbol{B}_{\mathrm{G}}(\boldsymbol{p},t)-\boldsymbol{B}(\boldsymbol{p},t)|/|\boldsymbol{B}(\boldsymbol{p},t)|$ of the field at $\boldsymbol{p}=(-0.5,-0.005,0)$ calculated at (*a*) $R_{\mathrm{m}}=10^5$ and (*b*) $R_{\mathrm{m}}=10^6$ using the exact Wiener bundle method and the approximate Gaussian method.

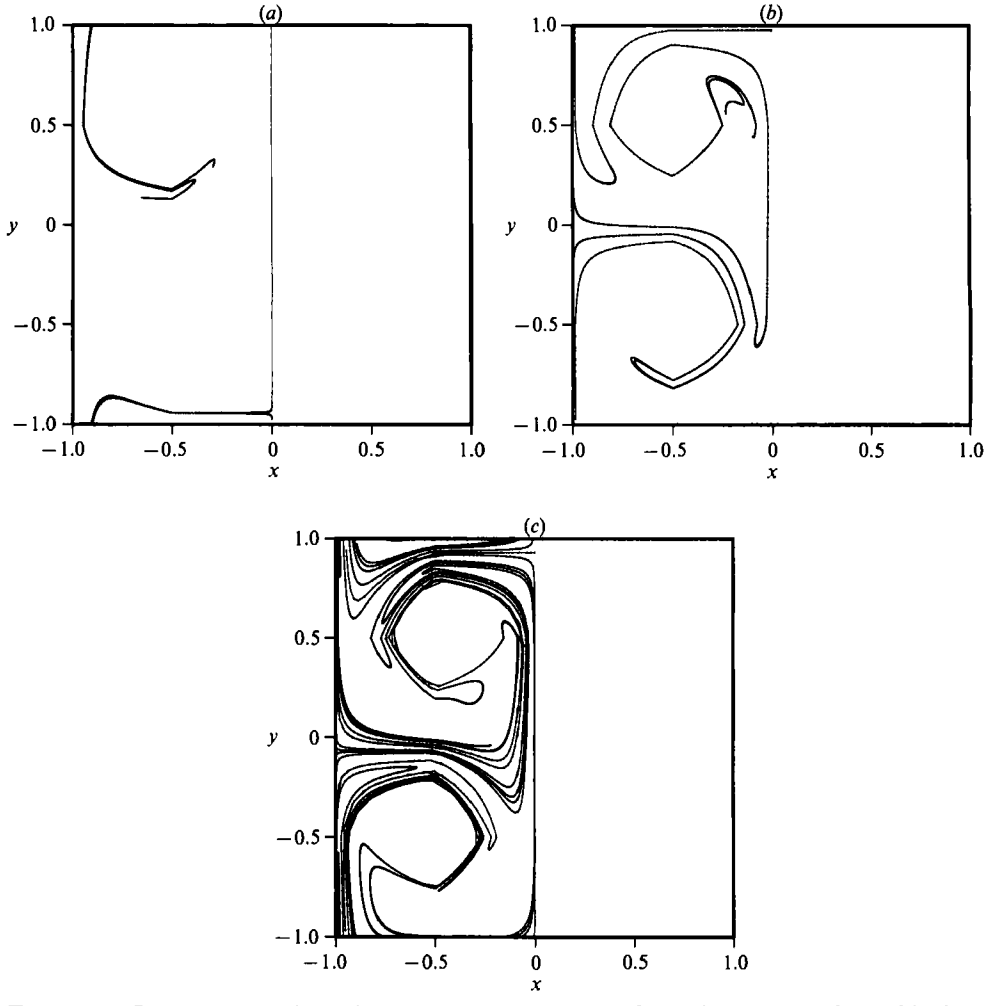

FIGURE 11. Line segment through $\boldsymbol{p} = (-0.5, -0.005, 0)$ of length 0.0192 in the stable direction advected backwards for times (*a*) $t = 12$, (*b*) $t = 17$, and (*c*) $t = 22$. $R_m = 10^5$.

Proctor for helpful comments, and the staffs of the Department of Applied Mathematics and Theoretical Physics, Cambridge, and the Department of Mathematics and Statistics, Newcastle, for their hospitality. Some of the calculations were done using an Encore multimax 520, a 14 processor parallel machine at the Newcastle University computing centre. This work was supported by a Fulbright grant and by NSF grants ATM-9011772 and DMS-8922676.

Appendix. Shadowing and the chaotic advection of vectors

The aim of this Appendix is to extend previously developed theory for the chaotic advection of scalars in the presence of small diffusion to the case of the vectors. It will be assumed that the chaotic system is an area-preserving two-dimensional map for which the shadowing principle holds, although the results hold for flows and higher dimensions as well. The idea is to substitute exact trajectories for Wiener trajectories and then relate the Wiener bundle solution to the Cauchy solution.

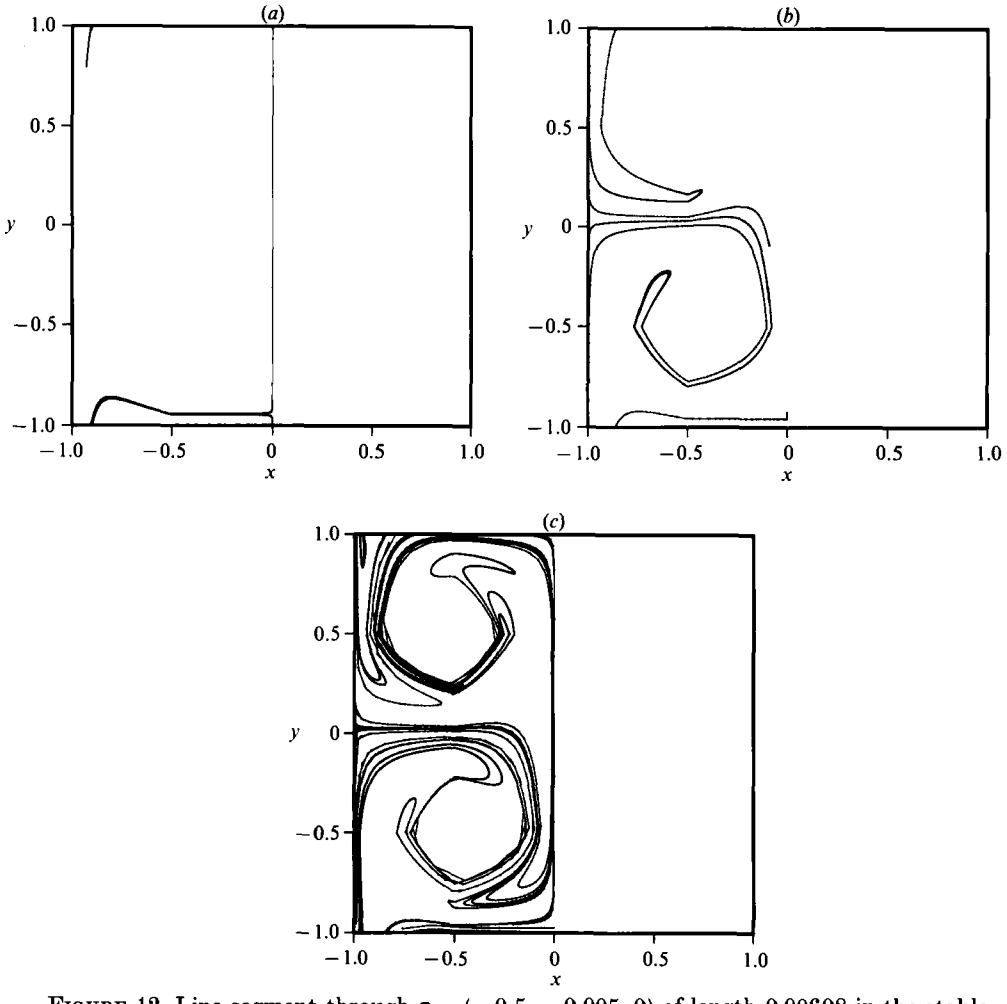

FIGURE 12. Line segment through $\boldsymbol{p} = (-0.5, -0.005, 0)$ of length 0.00608 in the stable direction advected backwards for times (*a*) $t = 12$, (*b*) $t = 18$, and (*c*) $t = 24$. $R_m = 10^6$.

This procedure was previously applied in Klapper (1992) to the problem of the advection of scalars in hyperbolic flows and maps under the equation

$$\frac{\partial \theta}{\partial t} + \boldsymbol{u} \cdot \nabla \theta = \mathscr{D} \nabla^2 \theta$$

where $\mathscr{D}$ is the scalar diffusivity. There it was found that the Wiener bundle arriving at a point $\boldsymbol{p}$ can be shadowed by a bundle of exact orbits arriving along the stable direction of $\boldsymbol{p}$ with density

$$\rho(y) = (2\pi\sigma^2)^{-\frac{1}{2}} \exp[-y^2/2\sigma^2]\,dy, \tag{A 1}$$

where y is the distance from $\boldsymbol{p}$ along the stable direction and the variance σ^2 is given by

$$\sigma^2 = 2\mathscr{D} \sum_{j=0}^{\infty} \lambda_{(-j)}^{2j}. \tag{A 2}$$

Here $\lambda_{(-j)}$ is the contraction rate of $\boldsymbol{f}^{-j}(\boldsymbol{p})$ in the stable direction. The direction of small-scale structure is the adjoint stable direction (see Klapper 1992) which, while in general not the same as the stable direction, is never perpendicular to it. Hence, for scalars at least, averaging over the Wiener bundle is equivalent to averaging over the small scales created in the $\mathscr{D} = 0$ problem. Vector advection is complicated by the fact that, unlike for scalars, the solution to the problem (3), where $\mathscr{D} = R_{\mathrm{m}}^{-1}$ (i.e. the Cauchy solution) relies not only on the initial conditions but also on details of the trajectory history through dependence on the Jacobian. Hence it should be verified that, for finite time anyway, the average of the Cauchy solution over the above-described bundle of exact trajectories indeed is a good approximation to the average over the Wiener bundle. That is, it needs to be shown that the history of a shadowing trajectory gives a good representation of the history of a Wiener trajectory.

To accomplish this, let $\boldsymbol{f}\colon \Omega \to \Omega$ be a map with the shadowing property. Given a point $\boldsymbol{p}$ consider an ϵ pseudo-trajectory $\{\boldsymbol{y}_i\}$, $-n \leqslant i \leqslant 0$, and a corresponding δ shadowing exact trajectory $\{\boldsymbol{x}_i\}$, $-n \leqslant i \leqslant 0$, such that $\boldsymbol{y}_0 = \boldsymbol{p}$. Thus

$$|\boldsymbol{x}_i - \boldsymbol{y}_i| < \delta, \quad -n \leqslant i \leqslant 0.$$

Assume that the initial conditions $\boldsymbol{B}_{-n}(\boldsymbol{x}) \equiv B(\boldsymbol{x}, n)$ are C^0 and $\boldsymbol{f}$ is C^2. Then $\boldsymbol{B}_{-n}$ and $\mathrm{D}\boldsymbol{f}$, the Jacobian of $\boldsymbol{f}$, are uniformly continuous if Ω is compact. Let $\mathrm{D}\boldsymbol{f}^n(\boldsymbol{x}_{-n})$, $\mathrm{D}\boldsymbol{f}_\epsilon^n(\boldsymbol{y}_{-n})$ be the Jacobians of $\boldsymbol{f}$ calculated along the trajectories $\{\boldsymbol{x}_i\}$, $\{\boldsymbol{y}_i\}$ respectively. Thus, for δ small and some constant C_n depending on n,

$$\begin{aligned}
\mathrm{D}\boldsymbol{f}^n(\boldsymbol{x}_{-n}) &= \mathrm{D}\boldsymbol{f}(\boldsymbol{x}_{-1})\,\mathrm{D}\boldsymbol{f}(\boldsymbol{x}_{-2}) \ldots \mathrm{D}\boldsymbol{f}(\boldsymbol{x}_{-n}),\\
\mathrm{D}\boldsymbol{f}_\epsilon^n(\boldsymbol{y}_{-n}) &= \mathrm{D}\boldsymbol{f}(\boldsymbol{y}_{-1})\,\mathrm{D}\boldsymbol{f}(\boldsymbol{y}_{-2}) \ldots \mathrm{D}\boldsymbol{f}(\boldsymbol{y}_{-n})\\
&= \mathrm{D}\boldsymbol{f}^n(\boldsymbol{x}_{-n}) + A\delta,
\end{aligned}$$

for a uniformly bounded $|A| \leqslant C_n$ since $\mathrm{D}\boldsymbol{f}$ is uniformly continuous and $\{\boldsymbol{x}_i\}$ δ shadows $\{\boldsymbol{y}_i\}$. Now since $\boldsymbol{B}_{-n}$ is uniformly continuous then $\boldsymbol{B}_{-n}(\boldsymbol{y}_{-n}) = \boldsymbol{B}_{-n}(\boldsymbol{x}_{-n}) + \boldsymbol{b}\delta$ for some bounded $\boldsymbol{b}$. Thus the magnetic fields contributed by the two trajectories are

$$\begin{aligned}
\boldsymbol{B}(\boldsymbol{x}_0, 0) &= \mathrm{D}\boldsymbol{f}^n(\boldsymbol{x}_{-n})\,\boldsymbol{B}_{-n}(\boldsymbol{x}_{-n}),\\
\boldsymbol{B}(\boldsymbol{y}_0, 0) &= (\mathrm{D}\boldsymbol{f}^n(\boldsymbol{x}_{-n}) + A\delta)\,(\boldsymbol{B}_{-n}(\boldsymbol{x}_{-n}) + \boldsymbol{b}\delta)\\
&= \mathrm{D}\boldsymbol{f}^n(\boldsymbol{x}_{-n})\,\boldsymbol{B}_{-n}(\boldsymbol{x}_{-n}) + O(\delta).
\end{aligned}$$

Hence it can be expected that the trajectories $\{\boldsymbol{x}_i\}$ and $\{\boldsymbol{y}_i\}$ will give similar contributions to the final magnetic field as $\mathscr{D}$ and thus $\delta \to 0$. Note that in our case $\delta \sim O(\epsilon) \sim O(R_{\mathrm{m}}^{-\frac{1}{2}})$.

As a final note it should be pointed out that the chaotic helical cell flow does not meet the conditions imposed because the flow Jacobian is not continuous across the planes $x = 0.5 + n$ and $y = 0.5 + m$ (see §4). However these are sets of measure 0 and hence as $\mathscr{D}$ vanishes they will have an increasingly negligible effect. Indeed the previous theorem could be extended to the case that $\mathrm{D}\boldsymbol{f}$ is not continuous on a set of measure 0 as long as $\mathrm{D}\boldsymbol{f}$ is bounded in a neighbourhood of that set.

REFERENCES

ARNOL'D, V. I. & AVEZ, A. 1968 *Ergodic Problems of Classical Mechanics*. New York: W. A. Benjamin.

ARNOL'D, V. I., ZELDOVICH, YA. B., RUZMAIKIN, A. A. & SOKOLOV, D. D. 1981 A magnetic field in a stationary flow with stretching in Riemannian space. *Zh. Eksp. Teor. Fiz.* **81**, 2052. (Transl. *Sov. Phys. JETP* **81**, 1083–1086.

BACKUS, G. 1958 A class of self-sustaining dissipative spherical dynamos. *Ann. Phys.* **4**, 372–477.

BAYLY, B. J. 1986 Fast magnetic dynamos in chaotic flows. *Phys. Rev. Lett.* **57**, 2800–2803.

BAYLY, B. & CHILDRESS, S. 1988 Construction of fast dynamos using unsteady flows and maps in three dimensions. *Geophys. Astrophys. Fluid Dyn.* **44**, 207–240.

BAYLY, B. J. & CHILDRESS, S. 1989 Unsteady dynamo effects at large magnetic Reynolds numbers. *Geophys. Astrophys. Fluid Dyn.* **49**, 23–43.

CHORIN, J. C. 1973 Numerical study of slightly viscous flow. *J. Fluid Mech.* **57**, 785–796.

DRUMMOND, I. T., DUANE, S. & HORGAN, R. R. 1984 Scalar diffusion in simulated helical turbulence with molecular diffusivity. *J. Fluid Mech.* **138**, 75–91.

FINN, J. M., HANSON, J. D., KAN, I. & OTT, E. 1989 Do steady fast magnetic dynamos exist? *Phys. Rev. Lett.* **62**, 2965–2968.

FINN, J. M., HANSON, J. D., KAN, I. & OTT, E. 1991 Steady fast dynamo flows. *Phys. Fluids* B**3**, 1250–1269.

FINN, J. M. & OTT, E. 1988 Chaotic flows and fast magnetic dynamos. *Phys. Fluids* **31**, 2992–3011.

FINN, J. M. & OTT, E. 1990 The fast kinematic magnetic dynamo and the dissipationless limit *Phys. Fluids* B**2**, 916–926.

GILBERT, A. D. 1988 Fast dynamo action in the Ponomerenko dynamo. *Geophys. Astrophys. Fluid Dyn.* **44**, 214–258.

GILBERT, A. D. 1991 Fast dynamo action in a steady flow. *Nature* **350**, 483–485.

GILBERT, A. D. 1992 Magnetic field evolution in steady chaotic flows. *Phil. Trans. R. Soc. Lond.* (in press).

GILBERT, A. D. & CHILDRESS, S. 1990 Evidence for fast dynamo action in a chaotic web. *Phys. Rev. Lett.* **65**, 2133–2136.

GREBOGI, C., HAMMEL, S. M., YORKE, J. A. & SAUER, T. 1990 Shadowing of physical trajectories in chaotic dynamics: containment and refinement. *Phys. Rev. Lett.* **65**, 1527–1530.

GUCKENHEIMER, J. & HOLMES, P. 1983 *Nonlinear Oscillations, Dynamical Systems, and Bifurcations of Vector Fields.* Springer.

KLAPPER, I. 1991 Fast magnetic dynamos. Dissertation, Courant Institute of Mathematical Sciences.

KLAPPER, I. 1992 Shadowing and the role of small diffusivity in the chaotic advection of scalars *Phys. Fluids* A (to appear).

KRAICHNAN, R. H. 1976 Diffusion of passive-scalar and magnetic fields by helical turbulence. *J. Fluid Mech.* **77**, 753–768.

LICHTENBERG, A. J. & LIEBERMAN, M. A. 1983 *Regular and Stochastic Motion.* Springer.

MCKEAN, H. P. 1969 *Stochastic Integrals.* Academic.

MOLCHANOV, S. A., RUZMAIKIN, A. A. & SOKOLOV, D. D. 1985 Kinematic dynamo action in a random flow. *Usp. Fiz. Nauk.* **145**, 593. (Transl. *Sov. Phys. Usp.* **28**, 307–326).

NEWHOUSE, S. 1980 Lectures on dynamical systems. In *Dynamical Systems.* (ed. J. Coates & S. Helgason). CIME Lectures. Boston: Birkhauser.

NEWHOUSE, S. 1986 In *The Physics of Phase Space.* (ed. Y. S. Kim & W. W. Zachary), pp. 2–8. Springer.

OTANI, N. J. 1988 Computer simulation of fast kinematic dynamos. *E.O.S. Trans. Am. Geophys. Union* **69**, No. 44, Abstract Sh51-15, p. 1366.

ROBERTS, G. O. 1972 Dynamo action of fluid motions with two-dimensional periodicity. *Phil. Trans. R. Soc. Lond.* A**271**, 411–454.

ROBERTS, P. H. & SOWARD, A. M. 1992 Dynamo theory. *Ann. Rev. Fluid Mech.* (to appear).

SOWARD, A. M. 1987 Fast dynamo action in a steady flow. *J. Fluid Mech.* **180**, 267–295.

VAINSHTEIN, S. I. & ZELDOVICH, YA. B. 1972 Origin of magnetic fields in astrophysics. *Sov. Phys. Usp.* **15**, 159–172.

VISHIK, M. M. 1989 Magnetic field generation by the motion of a highly conducting fluid. *Geophys. Astrophys. Fluid Dyn.* **48**, 151–167.

YOMDIN, Y. 1987 Volume growth and entropy. *Israel J. Maths* **57**, 285–300.